THE ASTROPHYSICAL JOURNAL, 462:740–745, 1996 May 10

H_2O AND OH MASERS AS PROBES OF THE OBSCURING TORUS IN NGC 1068

J. F. GALLIMORE,[1,2] S. A. BAUM,[1] C. P. O'DEA,[1] E. BRINKS,[3] AND A. PEDLAR[4]

Received 1995 August 30; accepted 1995 October 17

ABSTRACT

We report the discovery of OH masers and positionally resolved H_2O maser emission in the nucleus of NGC 1068. The brightest H_2O masers are associated with the radio continuum component that is probably the location of the central engine (Gallimore, Muxlow, and coworkers). These masers trace a ~ 50 mas (~ 5 pc), roughly linear velocity gradient along P.A. $94° \pm 4°$, which is almost at right angles to the local radio jet axis. The kinematics of the masers are well described as an edge-on Keplerian disk surrounding a large central mass concentration (black hole?). The inner radius of the maser disk is $\gtrsim 1.3$ pc, and the outer radius is ~ 2.5 pc, assuming a distance of 22 Mpc. The mass within the inner radius, normalized to the best-fit disk parameters, is $4.4 \times 10^7\ M_\odot \times (r_{\rm in}/1.3\ {\rm pc})\ (v_{\rm max}/378\ {\rm km\ s^{-1}})^2$. These masers might occur in the parsec-scale torus thought to obscure the central engine. Radio continuum emission fills the region interior to the H_2O masers, in agreement with the prediction that the continuum emission is thermal free-free radiation from the inner face of the molecular torus (Gallimore and coworkers).

The location of the OH masers and nuclear H I absorption (Gallimore and coworkers), measured with $\sim 1''$ angular resolution, is consistent with the location of the H_2O masers associated with the central engine. The H I absorption profile is also consistent with the Keplerian model for the H_2O maser disk kinematics, and the velocity range of the OH masers is similar to that spanned by both the H I and H_2O spectral features. It therefore seems likely that the OH masers and H I absorption also originate in the obscuring material surrounding the central engine. The OH masers indicate the presence of a more tenuous molecular medium in the torus, in addition to the denser material traced by the H_2O maser emission.

We have also discovered fainter H_2O masers located $0''.3$ (~ 30 pc) downstream along the radio jet. These masers are too distant from the central engine to arise in a parsec-scale torus. They may instead occur at the shock interface between the radio jet and an intervening molecular cloud. The implication is that H_2O magamaser emission may probe both circumnuclear disks and shock fronts in other active galactic nuclei.

Subject headings: galaxies: active — galaxies: individual (NGC 1068) — galaxies: Seyfert — masers — radio lines: galaxies

1. INTRODUCTION

The archetypal hidden Seyfert type 1 nucleus of NGC 1068 is a source of luminous H_2O maser emission (Claussen & Lo 1986, hereafter [CL]; Claussen, Heligman, & Lo 1984, hereafter [CHL]). CL suggested that the H_2O masers might arise in a parsec-scale torus surrounding the central engine (see also Gwinn et al. 1993). This torus was originally proposed by Antonucci & Miller (1985; see Antonucci 1993 for a review) to explain the obscuration of emission from the broad-line region (BLR) and central engine. It is now popularly thought that luminous extragalactic masers might occur in a dense obscuring medium suggested to hide the BLR in other narrow-line AGNs (e.g., Braatz, Wilson, & Henkel 1995; Miyoshi et al. 1995; Neufeld, Maloney, & Conger 1994; Watson & Wallin 1994).

We report in this paper VLA[5] centimeter-wave spectral-line observations of the nucleus of NGC 1068. These data include new observations of the 1665/1667 MHz lines of OH and archival 22 GHz H_2O maser data; they were obtained to explore the kinematics and distribution of the atomic and molecular material as potential probes of the parsec-scale torus of NGC 1068.

This paper is organized as follows. In § 2 we briefly describe the data reduction and analysis. An overview of the results is presented in § 3, and the implications of these discoveries are discussed in § 4. In this paper, we adopt a distance of 22 Mpc to NGC 1068, corresponding to a scale of $1'' \approx 100$ pc. Where relevant, the distance scale will be denoted by $D_{22} \equiv D/22$ Mpc.

2. OBSERVATIONS AND DATA REDUCTION

In 1983 September (CL) and 1987 July Mark Claussen observed NGC 1068 with the VLA in A array operating at the redshifted 22 GHz spectral line of the H_2O molecule. The gain and bandpass calibrations were repeated using updated techniques. In particular, we improved the bandpass calibration and the phase self-calibration over that achieved by CL. We also used natural weighting during the Fourier-transform imaging, resulting in roughly a factor of 2 improvement in sensitivity, at the expense of only roughly a 50% degradation of the angular resolution. In both runs, the velocity resolution is 10.6 km s^{-1}, and the observations alternated between two frequency bands, corresponding to $\Delta v = -400$ to -80 km s^{-1} and $\Delta v = 0$ to 300 km s^{-1}, where $\Delta v \equiv v - v_{\rm sys}$, and $v_{\rm sys} = 1150$ km s^{-1}

[1] Space Telescope Science Institute, 3700 San Martin Drive, Baltimore, MD 21218.
[2] Department of Astronomy, University of Maryland, College Park, MD 20742.
[3] National Radio Astronomy Observatory, P.O. Box O, Socorro, NM 87801-0387.
[4] National Radio Astronomy Laboratories, Jodrell Bank, Macclesfield, Cheshire, UK, SK11 9DL.
[5] The VLA is operated by the National Radio Astronomy Observatory which is operated by Associated Universities, Inc., under cooperative agreement with the National Science Foundation.

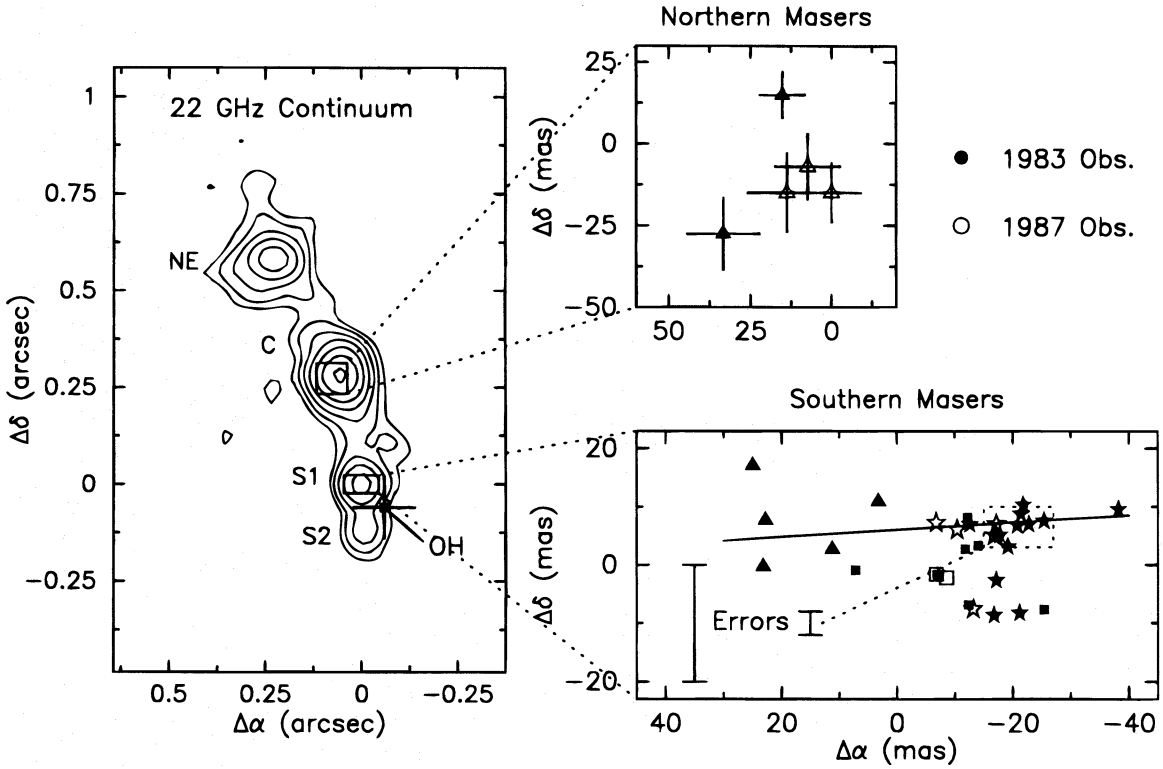

FIG. 1.—Location of the H_2O and OH masers relative to the 22 GHz radio continuum components (NE, C, S1, and S2; Papers I and II). Velocity ranges of the H_2O masers are coded by the following symbols: *stars*: $\Delta v > +100$ km s^{-1}; *squares*: $-100 < \Delta v \leq +100$ km s^{-1}; *triangles*: $\Delta v \leq -100$ km s^{-1}. Closed (open) symbols represent data from the 1983 (1987) observations. Error bars indicate the relative positional errors between maser spots. Error bars are plotted at the positions of the OH and northern masers, and the maximum positional errors for the southern masers are indicated in the lower left-hand corner of the southern masers panel. The smaller error bar pertains to the redshifted masers outlined by the dotted box. The best-fit orientation of the southern masers based on the Keplerian model (P.A. = 94°; § 4) is displayed as a solid line.

(Brinks et al. 1992). The rms image noise is 11 mJy per 0.″11 (FWHM; naturally weighted) beam channel^{-1}.

Two of the four principal radio continuum components were detected free of line emission on channel-averaged images (components NE and C; see Fig. 1). The positions of the masers were measured relative to these two continuum components for comparison with a 22 GHz continuum image (from Gallimore et al. 1996b, hereafter [Paper I]). The uncertainty between the maser and continuum positions is ~6 mas, based on the signal-to-noise ratio of the continuum components on the channel-averaged spectral line images. We subtracted the registered CLEAN-component model of an A-array 22 GHz continuum image (from Paper I) from the spectral line visibilities prior to the final Fourier-transform imaging and CLEAN deconvolution.

Observations of the OH 1665/1667 MHz main-line transitions were obtained with the VLA in A array. The data reduction procedures are discussed in Paper I. The Doppler velocity resolution is 35.5 km s^{-1}, referenced to the 1667 MHz line, and the rms image noise is 0.5 mJy per 1.″4 beam channel^{-1}. The position of the OH emission, relative to the subarcsecond jet structure, was determined by cross-correlating the line-free channel-averaged continuum image with a 1.7 GHz MERLIN continuum image (from Paper I).

3. RESULTS

In Figure 1 we plot the positions of significant H_2O and OH emission from individual channel maps relative to a 22

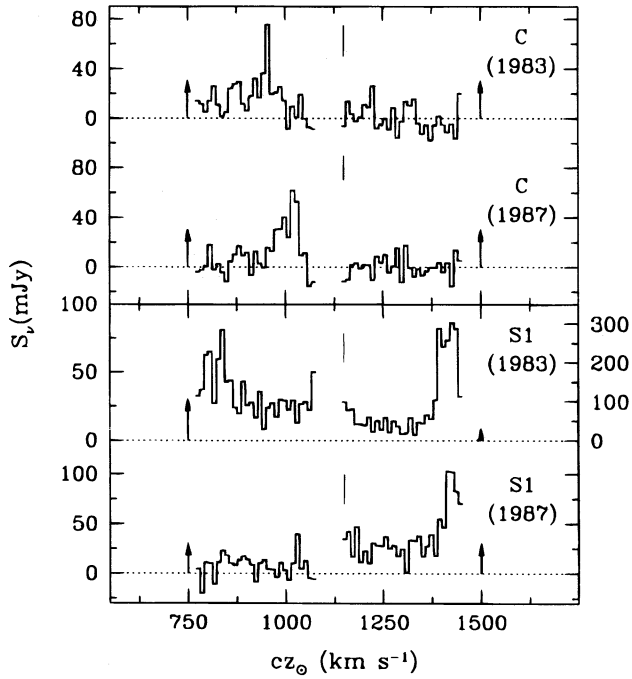

FIG. 2.—H_2O spectra of radio continuum component C (*top two spectra*) and subcomponent S1 (*lower two spectra*) from the 1983 and 1987 observations. Vertical arrows indicate the 3 σ level for a single channel, and vertical bars mark the systemic velocity of 1150 km s^{-1}. The vertical scale of the (1983) redshifted H_2O maser spectrum has been compressed for presentation.

TABLE 1

MASER PROPERTIES

Masers (1)	Epoch (2)	Δv (min, max) (km s^{-1}) (3)	L ($L_\odot$) (4)	T_b (10^4 K) (5)	Δv (km s^{-1}) (6)
Southern H_2O	1983	0, +297	308 ± 6	640	+276
	1987	0, +297	126 ± 6	25	+265
	1983	−375, −78	114 ± 6	12	−312
Northern H_2O	1983	−280, −195	27 ± 3	11	−195
	1987	−174, −121	26 ± 3	5.7	−131
Narrow OH.....	1994	−333, −262	0.32 ± 0.02	1.8	−298
Broad OH	1994	+20, +411	0.51 ± 0.03	0.55	+91

NOTE.—Explanation of columns: (1) group name; (2) epoch of observation; (3) velocity range; (4) integrated isotropic luminosity; (5) lower limit to the peak brightness temperature based on a 3 σ upper limit for the source diameter; (6) velocity at the peak. OH velocities are referenced to the 1667 MHz line. All velocities are relative to v_{sys} = 1150 km s^{-1}.

GHz continuum image (from Paper I), and in Figure 2 the H_2O maser spectra at the positions of the locally brightest emission. Basic spectral properties of the H_2O masers are summarized in Table 1. Because individual maser spots are not resolved with the VLA beam, the plotted positions are actually an intensity-weighted average over the maser spots, within the beam, and over a 10.6 km s^{-1} velocity range (i.e., the channel width).

The naming of the principal continuum features (NE, C, S1, and S2) in Figure 1 follows the convention used in Paper I and Gallimore et al. (1996a, hereafter Paper II). Based on the radio continuum spectra, we have interpreted components NE and C as knots in the radio jet (Paper II). There is evidence that component C occurs at a shock interface with a molecular cloud (Paper II). Component S1 is the most likely candidate for the central engine because its centimeter-wave spectrum is inverted (Paper II; Muxlow et al. 1995). The brightness temperature ($\sim 10^5$ K) is too low for synchrotron self-absorption, therefore we have suggested that most of the emission is due to thermal free-free radiation (Paper II).

CL detected only the brighter redshifted and near-systemic H_2O masers located at component S1 (hereafter the "southern masers"). They found that the velocity-averaged positions of the southern masers are not resolved with their calibration. With our improved calibration and

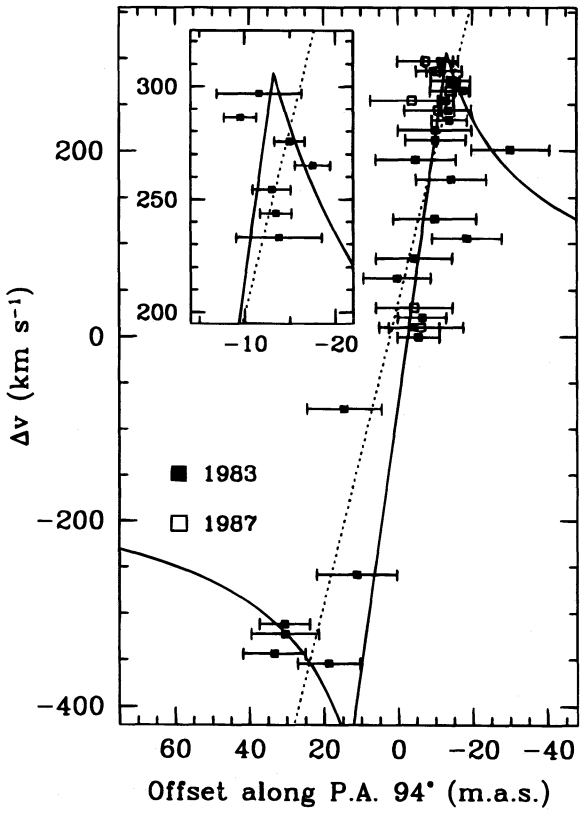

FIG. 3.—Position–velocity diagram of the southern H_2O masers. The solid line is the Keplerian rotation curve fit, and the dotted line is the linear rotation curve fit. A closeup of the (1983) positions of the bright redshifted masers is plotted in the inset.

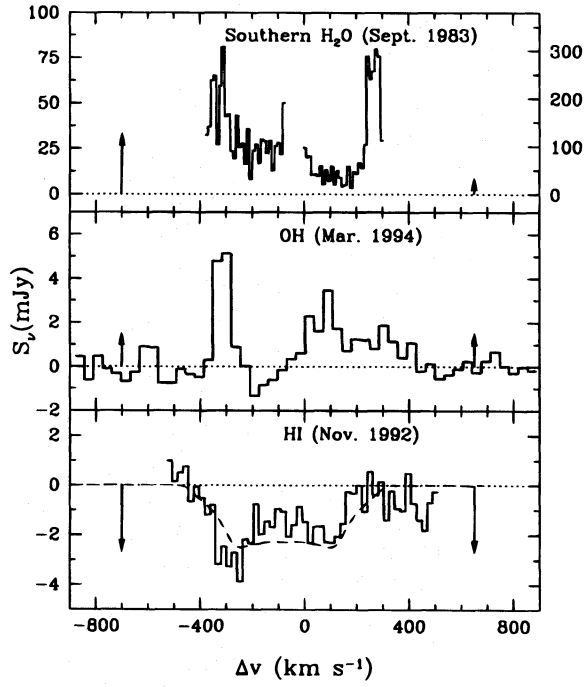

FIG. 4.—Comparison of the southern H_2O (1.35 cm), OH (18 cm), and H I (21 cm) line spectra of the nucleus of NGC 1068. Vertical arrors indicate the 3 σ level for a single channel. Velocities are relative to v_{sys} = 1150 km s^{-1}. The vertical scale of the redshifted H_2O maser spectrum has been compressed for presentation. The dashed line is the predicted H I absorption profile of a uniform Keplerian annulus described by the best-fit values in Table 2, assuming that it is uniformly illuminated by 21 cm continuum at its inner radius. The predicted profile was scaled to the mean depth of the H I absorption line, but the profile shape is determined solely by the maser rotation curve fit.

imaging, we have obtained three principal results not found in the analysis of CL. First, we have detected the blueshifted H_2O masers originally detected in the single-dish spectrum of CHL. Second, there is a significant trend in the southern maser positions as a function of velocity (Fig. 3). Third, we have detected blueshifted H_2O masers associated with component C (hereafter the "northern masers").

We have also detected 1665/1667 MHz line emission associated with the southern radio double (components S1 and S2; see Fig. 1). The OH emission spectrum, in comparison with the 1983 H_2O spectrum and the nuclear H I absorption spectrum (Gallimore et al. 1994), is presented in Figure 4. Spectral properties of the OH emission lines are included in Table 1.

4. DISCUSSION

4.1. *The Southern H_2O Masers*

The brightest H_2O maser emission is unambiguously associated with component S1 (Fig. 1; cf. CL), which is the most likely location of the central engine (Papers I and II; Muxlow et al. 1996). The rotation curve of the southern masers is roughly linear on ~ 10 mas ($\sim$ parsec) scales (Fig. 3), and the high-velocity features are nearly symmetric about v_{sys} (cf. CL; CHL). The simplest explanations for the maser kinematics are therefore (1) a nearly edge-on, rotating disk surrounding the central engine, or (2) a bipolar outflow driven by the central engine. The latter option seems unlikely since the orientation of the masers is nearly at right angles to the radio jet axis (P.A. = 11°; Paper I). On the other hand, based on evidence from spectropolarimetry, imaging polarimetry, and X-ray spectroscopy, the central engine in NGC 1068 is thought to be obscured by a dusty torus of molecular gas viewed nearly edge-on (cf. Capetti et al. 1995; Antonucci 1993 and references therein). We therefore consider a rotating disk or torus the more probable origin for the southern masers (e.g., Watson & Wallin 1994).

4.1.1. *Rotation Curve Fits*

Assuming a circularly rotating disk, we fitted both (1) a linear rotation curve, $v \propto r$, and (2) a Keplerian rotation curve for which $v \propto r^{-1/2}$ for $r \geq r_{min}$. The results are provided in Table 2. For simplicity, we assume that the disk is viewed exactly edge-on. The actual inclination is poorly constrained by these observations: $i = 79° \pm 16°$ based on the minor-axis separation between the near-systemic and high-velocity features. The implied inclination corrections are, however, small: $(1 - \sin i) = 2\% \pm 5\%$.

Of course, more sophisticated kinematics probably obtain in the obscuring material. Modifications that have been proposed include, for example, random motions induced by radiation pressure (Pier & Krolik 1992) and poloidal motions in centrifugally driven winds (Königl & Kartje 1994). Models that account for these effects require additional parameters (e.g., midplane column densities, midplane poloidal velocities, etc.). The reduced-χ^2 values for the rotation curve fits (Table 2) are already near unity, so the data at present do not warrant the inclusion of more parameters. As a result, we cannot, unfortunately, constrain the parameters of more sophisticated kinematics with the present data; sensitive VLBI observations will be necessary to constrain such models.

The Keplerian rotation curve provides a significantly better fit to the data than does the linear rotation curve. The two additional parameters (e.g., v_{sys}, r_{in}) are significant at the 0.2% level according to an F-test. We caution, however, that the presence of a Keplerian turnover is inferred statistically; the maser spots poorly sample the low-velocity tails of the best-fit rotation curve. Sensitive VLBI observations will be necessary to detect and image the turnover, and refine the numbers presented here. The caveat is that the quantities θ_{in} and v_{max} as they are described by the model fits are, at worst, lower limits to their true values. Nevertheless, as we demonstrate below, the best-fit parameters of the Keplerian turnover disk model are at least self-consistent with the predictions of the obscuring torus and the 21 cm H I absorption profile.

In Table 3 we summarize some basic properties of the central engine + torus system, based on the Keplerian disk model. We adopted the Pier et al. (1994) empirical spectrum of the AGN in NGC 1068. The luminosity of the central engine is normalized to f, the fraction of the central luminosity reflected into our sight line ($f \sim 0.01$; Pier et al. 1994 and references therein). The mass and column density of the maser disk are normalized to the volume filling fraction ϵ. We have also normalized those quantities that depend on the Keplerian turnover disk model to $\hat{\theta}_{in} \equiv \theta_{in}/13.5$ mas and $\hat{v}_{max} \equiv v_{max}/378$ km s^{-1} (see Table 2). The masers extend over a diameter of ~ 50 mas. Properties of the maser

TABLE 2

H_2O ROTATION CURVE FITS

Model	Parameter	Value
Linear.....	v/θ	16.1 ± 1.3 km s^{-1} mas^{-1}
	P.A.	$95° \pm 4°$
	χ^2(dof)	51.4 (44)
Kepler.....	θ_{in}	13.2 ± 1.9 mas
	v_{max}	378 ± 23 km s^{-1}
	v_{sys}	1078 ± 15 km s^{-1}
	P.A.	$94° \pm 4°$
	χ^2 (dof)	34.1 (42)
...	θ_h	3.5 ± 0.7 mas

NOTE.—The values of χ^2 are probably slightly underestimated due to an overestimate of the positional errors. The reported errors are 1 σ, derived from the $\Delta\chi^2 = 1$ surface in parameter space. The maser disk scale height, θ_h, is based on residual distances from the best-fit line to the maser source positions.

TABLE 3

PROPERTIES OF THE TORUS AND CENTRAL ENGINE

Property	Value	Normalization
r_{in}(disk) (pc)	1.3	$D_{22}\hat{\theta}_{in}$
r_{out}(disk) (pc)	2.5	$D_{22}\hat{\theta}_{out}$
h (pc).....	0.35	$D_{22}\hat{\theta}_h$
Orbital period (yr).....	3.4×10^3	$D_{22}\hat{\theta}_{in}\hat{v}_{max}^{-1}\sin i$
$M(r < r_{in})$ ($M_\odot$).....	4.3×10^7	$D_{22}\hat{\theta}_{in}\hat{v}_{max}^2(\sin i)^{-2}$
M(disk) ($M_\odot$)	2.4×10^5	$D_{22}^2(\hat{\theta}_{out}^2 - \hat{\theta}_{in}^2)n_{10}\hat{\theta}_h\epsilon_{(-4)}$
L_{bol}[a] (ergs s^{-1})	8.4×10^{44}	$D_{22}^2(f_{(-2)})^{-1}$
L_{bol}/L_E (%)	19	$D_{22}\hat{\theta}_{in}^{-1}\hat{v}_{max}^{-2}(\sin i)^2(f_{(-2)})^{-1}$
N_H(disk) (cm^{-2})	7.0×10^{24}	$D_{22}(\hat{\theta}_{out} - \hat{\theta}_{in})n_{10}\epsilon_{(-4)}$

NOTE.—Properties of the central engine and maser disk (torus?) inferred from the Keplerian model and the maser observations. Definitions of the normalization parameters are provided in the text (§ 4). Here $n_{10} = n/10^{10}$ cm^{-3}, $f_{(-2)} = f/0.01$, $\epsilon_{(-4)} = \epsilon/10^{-4}$, $\hat{\theta}_h \equiv \theta_h/3.5$ mas, where θ_h is the angular scale height of the maser disk and L_E is the Eddington luminosity.

[a] Pier et al. 1994.

disk are therefore normalized by $\hat{\theta}_{out} \equiv 25$ mas. We also estimated the scale height, h, of the maser disk by measuring the variance-weighted, rms distance of the masers to the best-fit line to the maser positions. Because the disk might be slightly inclined, this estimate is actually an upper limit to the disk scale height.

The interior mass is $M(r \lesssim 1.3 \text{ pc}) \sim 4 \times 10^7\ M_\odot \times [D_{22}\ \hat{\theta}_{in}\ \hat{v}^2_{max}(\sin i)^{-2}]$. Although we will not discuss the possible nature of such a large mass concentration (lucid arguments are presented in Maoz 1995 and Miyoshi et al. 1995), we note that the rotation curve is consistent with the presence of a massive, compact object (black hole?) that may act as the central engine (e.g., Rees 1984). It is difficult to imagine that such a large mass concentration might be associated with anything besides the central engine, so the maser rotation curve provides at least self-consistent evidence that component S1 is the location of the central engine.

Gwinn et al. (1993), using a VLBI phase gradient technique, measured an upper limit to the mas-scale velocity gradient of the brightest maser emission, using a VLBI phase gradient technique. The 1 σ upper limit they derived is 190 km s^{-1} mas^{-1} (1900 D_{22} km s^{-1} pc^{-1}). We measure a 10 mas-scale velocity gradient of 16–29 km s^{-1} mas^{-1}, consistent with the Gwinn et al. upper limit.

4.1.2. *The Relation to the Obscuring Torus Model*

The Keplerian disk model agrees in two ways with the predictions for the obscuring torus. First, spectropolarimetry predicts that the plane of the torus orients along P.A. = 87° ± 2° (on subarcsecond scales; Antonucci, Hurt, & Miller 1994), in close agreement with the maser disk, P.A. = 94° ± 4°. Second, the column density through the disk must be $\sim 10^{25}$ cm^{-2} to explain the attenuation of hard X-rays (e.g., Mulchaey, Mushotzky, & Weaver 1992). H_2O masers probe gas densities $n(H_2) > 10^7$ cm^{-3} (e.g., Watson 1994). The width of the maser region is ~ 1 pc, so the column through the maser region is greater than $6 \times 10^{25}\ \epsilon$ cm^{-2}, in agreement with the X-ray inferred column. More generally, the column density through the H_2O maser region alone is sufficient to block hard X-rays, provided $(n/10^7 \text{ cm}^{-3})\epsilon \gtrsim 0.2$.

In Paper II, we suggested that the inverted radio continuum spectrum and low brightness temperature of subcomponent S1 might be due to opaque thermal free-free radiation from a photoevaporating zone (PZ) at the inner surface of the torus (see also Pier & Voit 1995; Neufeld et al. 1994; Krolik & Lepp 1989). The prediction is that the continuum source (S1) and maser ring diameters should agree. The size of the maser region is ~26–50 mas, in good agreement with the measured continuum source diameter, 40 ± 5 mas (Paper I). More evidence for the PZ is provided by the H I absorption profile. We computed the profile that would be expected if the H I absorption were to arise in the Keplerian maser disk (Table 2). We assumed for simplicity that the atomic gas is uniform and that the inner surface of the torus is uniformly illuminated by 1.4 GHz continuum (i.e., opaque free-free radiation). Shown in Figure 4, there is a surprisingly good agreement between the shape of the observed H I absorption spectrum and the profile predicted by this simplified torus + PZ model. An interesting consequence is that the southern H_2O masers may be amplifying thermal free-free emission from the PZ, in addition to (or rather than) nonthermal radio emission from the central engine. VLBI observations will be required to determine the dominant continuum source.

The measured scale height of the maser disk, $h_{1/2} \lesssim 0.2$ pc, is small relative to the lower limit on the inner radius, $r_{in} \gtrsim 1.3$ pc. The half-opening angle of the maser disk is correspondingly very broad, $\theta_{1/2} \gtrsim 82°$. To ensure that the central engine is obscured by the parsec-scale disk, the disk must be highly inclined, $i \gtrsim 82°$, if the masers trace the vertical distribution of the obscuring material surrounding the central engine. It seems more likely that the disk is instead stratified in the vertical direction, such that the masers only trace material very close to the midplane. For example, vertical stratification is predicted in the wind model of Königl & Kartje (1994). Alternatively, the maser disk might be heated from above by X-radiation. Such heating would restrict the vertical distribution of H_2O masers to a shielded region near the midplane (Neufeld & Maloney 1995). Sources of X-radiation might be the central engine viewed obliquely by the disk (requiring the presence of a warp in the disk; Neufeld & Maloney 1995) or X-rays reflected onto the disk by a scattering halo surrounding the disk.

4.1.3. *Comparison with NGC 4258*

The mass of the central engine in NGC 1068 is close to that in NGC 4258 ($3.6 \times 10^7\ M_\odot$; Miyoshi et al. 1995). However, assuming that both engines emit isotropically, the central engine in NGC 1068 is much more luminous than NGC 4258: $\tilde{L}_X \sim 750(f/0.01)^{-1}$ in 2–10 keV X-rays (Makishima et al. 1994; Marshall et al. 1993), where we adopt the notation $\tilde{x} \equiv x(\text{NGC 1068})/x(\text{NGC 4258})$. This ratio implies a swifter infall rate to the central engine in NGC 1068: $\dot{M}_{disk}(\text{NGC 1068}) \sim 750\ \dot{M}_{disk}(\text{NGC 4258})$ (see also Neufeld & Maloney 1995). This is a lower limit to the ratio of the infall rates because an X-ray–heated wind in NGC 1068 may remove an additional $\sim 1\ M_\odot$ yr^{-1} from the torus (Krolik & Begelman 1986). Presumably, the dynamics of the parsec-scale disk of NGC 1068 must be very different from those in NGC 4258 to explain the relatively prodigious fueling rate, but the present data have insufficient spatial resolution to explore the dynamics in such detail.

Another interesting difference is that the inner radius of the disk in NGC 1068, $1.3 \pm 0.2\ D_{22}$ pc, is a factor $(10 \pm 2)D_{22}$ times larger than the inner radius in NGC 4258 (Miyoshi et al. 1995). The difference in the sizes of the maser annulli in NGC 1068 and NGC 4258 might be explained by X-ray heating of the molecular disk. The inner radius at which molecules can exist is determined by the X-ray flux received by the disk: $r_{in} \propto (L_X/N_H^{0.9}p)^{1/2}$, where N_H is the shielding column to the central engine and p is the local pressure (Neufeld et al. 1994). The predicted size ratio is then $\tilde{r}_{in} \sim 30 D_{22} N_H^{-0.45} \tilde{p}^{-0.5}(0.01/f)^{0.5}$. The agreement with the measured ratio, $\tilde{r}_{in} \sim 10 D_{22}$, is good considering the uncertainty in the measurement of f. The ratios can also be reconciled if $\tilde{N}_H^{0.9}\tilde{p} \sim 10$.

4.2. *The* OH *Masers*

The OH emission spectrum (Fig. 4) includes two significant features: (1) the "narrow" line, a relatively narrow peak centered near $\Delta v = -310$ km s^{-1}, and (2) the "broad" line, a broader but weaker feature covering the velocity range $\Delta v \sim 0$ to $+411$ km s^{-1} (velocities are referenced to the 1667 MHz line). The brightness temperature of the peak OH emission is ≳18,000 K, based on the 3 σ

upper limit to the source diameter. Shock- or X-ray heating might raise the temperature of molecular gas to such a high temperature, but OH would be relatively abundant only in regions at $T \lesssim 1000$ K (e.g., Neufeld et al. 1994; Hollenbach & McKee 1989). A simpler explanation, which we adopt, is that the OH emission is amplified by the maser process. The resolution and sensitivity of the 1.7 GHz data are insufficient to determine whether the OH masers coincide with the H_2O masers on subparsec scales, but we cannot rule this possibility out.

We identify the narrow line with the 1667 MHz transition at $\Delta v \sim -300$ km s^{-1} because of the velocity agreement with the blueshifted southern H_2O masers (Fig. 4; § 4.1). The broad OH line is more difficult to interpret since, in addition to 1667 MHz emission, it may include 1665 MHz emission corresponding to the narrow line (referenced to the 1667 MHz line, the velocity difference between the 1665 and 1667 MHz lines is ~ 350 km s^{-1}). However, the narrow 1665 MHz line should cover the velocity range $\Delta v \sim +20$ to $+90$ km s^{-1}, but the broad emission extends to $\Delta v \sim +411$ km s^{-1}. Therefore, there is probably a contribution from redshifted 1667 MHz emission, extending to a redshift of $\Delta v \lesssim +411$ km s^{-1}.

It seems likely that the OH masers and the H I absorption-line gas are also located in the rotating molecular disk because (1) their location is consistent with being cospatial with the southern H_2O masers, and (2) the Doppler velocity ranges are similar to that covered by the southern H_2O masers. Indeed, the H I absorption profile is consistent with the maser disk kinematics (Fig. 4; § 4.1). However, H_2O maser emission typically requires conditions (i.e., gas densities) that would quench OH maser emission (Elitzur 1992). Possible origins for the OH masers include a tenuous medium filling the space between denser, H_2O-masing cloudlets, or perhaps a dissociating envelope surrounding such cloudlets (cf. Neufeld & Maloney 1995). These ideas will be difficult to test because the sizes of individual cloudlets are probably $\ll 1$ mas at the distance of NGC 1068 (e.g., Pier & Voit 1995).

4.3. *The Northern* H_2O *Masers*

The northern masers are displaced $\sim 0\farcs3$ (~ 30 pc) along the radio jet, and so do not arise in the parsec-scale torus envisioned to hide the central engine. Rather, the northern H_2O masers coincide with component C (Fig. 1), the site of a possible shock interface between the radio jet and dense, near-nucleus gas at which the radio jet is diverted (Paper II). In analogy with less luminous interstellar H_2O masers, a possible explanation is that the masers occur in the shock-excited molecular gas. In this scenario, masers occur throughout the shock interface, but we would preferentially detect masers located in the tangent plane of the shock interface that is parallel to our sight line (e.g., Watson 1994). We speculate that the variability of the maser features is a consequence of the geometrical evolution of the shock front as the jet plows into the inhomogeneous cloud. To explain the inverted level populations of the H_2O molecules, we favor the dissocative shock scenario of Elitzur, Hollenbach, & McKee (1989), because the impinging radio jet is presumably hypersonic inside the molecular cloud. We are currently pursuing further observations to support a more detailed model of this shock scenario.

It is a pleasure to acknowledge discussions with Dave Axon, Alessandro Capetti, Reinhard Genzel, and Andrew Wilson, and the helpful suggestions and advice lent by Miller Goss, Carl Gwinn, Julian Krolik, David Neufeld, Huib van Langevelde, and Juan Uson. The referee, Ed Pier, provided suggestions which improved the presentation and tightened some of the arguments in this paper. We also thank Mark Claussen, who brought to our attention the archival (1987) H_2O maser data, and Meri Stanley, who assisted in translating the archival data to the newer standard format. J. F. G. received support from the STScI Director's Discretionary Fund during part of the course of this work. Further support for this work was provided by NASA through grant AR-04933.01-92A from the Space Telescope Science Institute, which is operated by the Association of Universities for Research in Astronomy, Inc., under NASA contract NAS 5-26555. This paper represents a portion of J. F. G.'s Ph.D. thesis, to be submitted in partial fulfillment of the requirements of the Graduate School of the University of Maryland.

REFERENCES

Antonucci, R. 1993, ARA&A, 31, 473
Antonucci, R., Hurt, T., & Miller, J. 1994, ApJ, 430, 210
Antonucci, R. R. J., & Miller, J. S. 1985, ApJ, 297, 476
Braatz, J. A., Wilson, A. S., & Henkel, C. 1994, ApJ, 437, L99
Brinks, E., Skillman, E. D., Terlevich, R. J., & Terlevich, E. 1992, BAAS, 24, 1275
Capetti, A., Axon, D. J., Macchetto, F., Sparks, W. B., & Boksenberg, A. 1995, ApJ, 446, 155
Claussen, M. J., Heiligman, G. M., & Lo, K.-Y. 1984, Nature, 310, 298 (CHL)
Claussen, M. J., & Lo, K.-Y. 1986, ApJ, 308, 592 (CL)
Elitzur, M. 1992, Astronomical Masers (Dordrecht: Kluwer)
Elitzur, M., Hollenbach, D. J., & McKee, C. F. 1989, ApJ, 346, 983
Gallimore, J. F., Baum, S. A., & O'Dea, C. P. 1996a, ApJ, in press (Paper II)
Gallimore, J. F., Baum, S. A., O'Dea, C. P., Brinks, E., & Pedlar, A. 1994, ApJ, 422, L13
Gallimore, J. F., Baum, S. A., O'Dea, C. P., & Pedlar, A. 1996b, ApJ, 458, 136 (Paper I)
Gwinn, C. R., Antonucci, R. R. J., Barvainis, R., Ulvestad, J., & Neff, S. 1993, in Subarcsecond Radio Astronomy, ed. R. J. Davis & R. S. Booth (Cambridge: Cambridge Univ. Press), 331
Hollenbach, D., & McKee, C. F. 1989, ApJ, 342, 306
Königl, A., & Kartje, J. F. 1994, ApJ, 434, 446
Krolik, J. H., & Begelman, M. C. 1986, ApJ, 308, 55
Krolik, J. H., & Lepp, S. 1989, ApJ, 347, 179
Makishima, K., et al. 1994, PASJ, 46, L77
Maoz, E. 1995, ApJ, 447, 91
Marshall, F. E., et al. 1993, ApJ, 405, 168
Miyoshi, M., Moran, J., Herrnstein, J., Greenhill, L., Nakai, N., Diamond, P., & Inoue, M. 1995, Nature, 373, 127
Mulchaey, J. S., Mushotzky, R. F., & Weaver, K. A. 1992, ApJ, 390, L69
Muxlow, T. W. B., Pedlar, A., Holloway, A., Gallimore, J. F. & Antonucci, R. R. J. 1996, MNRAS, in press
Neufeld, D. A., & Maloney, P. R. 1995, ApJ, 447, L17
Neufeld, D. A., Maloney, P. R., & Conger, S. 1994, ApJ, 436, L127
Pier, E. A., Antonucci, R., Hurt, T., Kriss, G., & Krolik, J. 1994, ApJ, 428, 124
Pier, E. A., & Krolik, J. H. 1992, ApJ, 399, L23
Pier, E. A., & Voit, G. M. 1995, ApJ, 450, 628
Rees, M. J. 1984, ARA&A, 22, 471
Watson, W. D. 1994, in The Structure and Content of Molecular Clouds, ed. T. L. Wilson & K. L. Johnston (Berlin: Springer), 109
Watson, W. D., & Wallin, B. K. 1994, ApJ, 432, L35